In-situ co-doping of sputter-deposited TiO$_2$:WN films for the development of photoanodes intended for visible-light electro-photocatalytic degradation of emerging pollutants

N. Delegan,[1] R. Pandiyan,[1] S. Komtchou,[2] A. Dirany,[2] P. Drogui,[2] and M. A. El Khakani[1,*]

[1]*Institut National de la Recherche Scientifique, Centre-Énergie, Matériaux et Télécommunications, 1650 Blvd. Lionel-Boulet, Varennes, QC J3X-1S2, Canada*

[2]*Institut National de la Recherche Scientifique, Centre-Eau, Terre et Environnement, 490 Rue de la Couronne, QC G1K-9A9, Canada*

*Corresponding author: elkhakani@emt.inrs.ca

Abstract

We report on the magnetron sputtering deposition of *in-situ* codoped TiO$_2$:WN films intended for electro-photocatalytic (EPC) applications under solar irradiation. By varying the RF-magnetron sputtering deposition parameters, we were able to tune the *in-situ* incorporation of both N and W dopants in the TiO$_2$ films over a wide concentration range (i.e. 0-9at.% for N and 0-3at.% for W). X-ray photoelectron spectroscopy analysis revealed that both dopants are mostly of a substitutional nature. The analysis of the UV-Vis transmission spectra of the films confirmed that the optical band-gap of both TiO$_2$:N and TiO$_2$:WN films can be significantly narrowed (from 3.2eV for undoped-TiO$_2$ down to ~2.3eV for the doped ones), by tuning their dopant concentrations. We were thus able to pinpoint an optimal window for both dopants (N and W) where the TiO$_2$:WN films exhibit the narrowest bandgap. Moreover, the optimal codoping conditions greatly reduce the recombination defect state density compared to the monodoped TiO$_2$:N films. These electronically passivated TiO$_2$:WN films are shown to be highly effective for the EPC degradation of atrazine (pesticide pollutant) under sunlight irradiation (93% atrazine degraded after only 30 min of EPC treatment). Indeed, the optimally codoped TiO$_2$:WN photoanodes were found to be more efficient than both the undoped-TiO$_2$ and equally-photosensitized TiO$_2$:N photoanodes (by ~70% and ~25%, respectively), under AM1.5 irradiation.

1 Introduction

2 Since the pioneering work of Fujishima and Honda in 1972 on titanium dioxide (TiO_2) water

3 splitting[1], the research on the photocatalytic properties of TiO_2 and its varied forms has continued

4 to attract great attention. In fact, TiO_2 offers a unique combination of unpaired features among which

5 are its wide bandgap and high chemical stability[1–5] in addition to its availability and affordability.

6 All these facts have made TiO_2 the candidate of choice for applications in solar energy

7 conversion[1,2,5] and photo-degradation of contaminants.[6,7]

8 Fundamentally, TiO_2 is an n-type semiconductor with a wide intrinsic bandgap (E_g) of 3.0 eV and

9 3.2 eV for rutile and anatase polymorphs, respectively. This inherently restricts the photoactivity of

10 titania based devices to the ultra-violet (UV) range (which represents only ~4% of the irradiance of

11 the sunlight) and limits to a certain extent its implementation in large scale industrial photo-

12 processes.[8] It is thus understandable that substantial research effort is aimed at extending the

13 photosensitivity of TiO_2 to the visible light range (which represents ~40% of solar irradiance)

14 through the narrowing of its bandgap via varied approaches including self-doping,[9] dye-

15 sensitization,[2,4] cationic doping,[4,7] and anionic doping.[3,4,6,7] For the latter approach, substitutional

16 nitrogen (N) doping has been shown to be very effective, as it leads to the formation of discrete N_{2p}

17 acceptor states within the E_g above the valence band maximum (VBM) reducing thereby the

18 bandgap energy from 3.2 eV (anatase) to ~2.3 eV (N-doped anatase).[4,6,7] In this context, we have

19 demonstrated in a previous study[7] that the *in-situ* N-doping induced E_g narrowing of sputtered TiO_2

20 films was directly correlated with the significant increase of their electro-photocatalytic (EPC)

21 capacity to degrade the chlortetracycline (CTC) contaminant under sunlight exposure. In fact, N

22 doping is a more complex process which induces different energy states within the semiconductor's

23 forbidden gap.[10–17] Some of these energy levels act as acceptor states within the E_g and therefore

1 effectively reduce the energy required for photoexcitation, while others act as charge traps and/or

2 recombination centers hindering thereby the photocharge transport. Notably, the introduction of N

3 into the TiO_2 lattice has been shown to lead to two types of these energy states associated with the

4 dopant being into substitutional or interstitial sites. The substitutional doping is associated with the

5 formation of N_{2p} acceptor levels just above the O_{2p} levels, whereas the interstitial one is related with

6 isolated N-O type deep gap states within the E_g that may act as photocharge recombination

7 centers.[10–15] In addition, the defects induced by the presence of both dopants are usually

8 compensated for by the oxide structure via the formation of oxygen vacancies (V_O), which in turn

9 act as potent recombination centers located beneath the conduction band minimum (CBM).[14,16] In

10 sum, both experimental and theoretical studies[10–17] indicate that mono-doping (with N for example)

11 while being very effective in narrowing the bandgap, it concomitantly creates recombination centers

12 that tend to reduce the extracted photogenerated current.[4,7] This limits the full exploitation of the

13 photocatalytic efficiency gain from the absorption edge red-shift.[5] To counteract this limitation,

14 density of states (DOS) models[18–24] have showed that it is possible to minimise the undesired side-

15 effects arising from N-doping by achieving an electronically passivated acceptor-donor co-doping

16 approach. The latter would suppress the charge defects acting as recombination centers, while

17 maintaining an enhanced visible light absorption.[5,18–21,23,24] By theoretically investigating different

18 dopant couples,[21,23] tungsten (W) and nitrogen (N) were identified as the most interesting pair that

19 would narrow the E_g while minimizing the recombination of photogenerated excitons through

20 electronic passivation of uncompensated charges.[18–20,22] Recent chemical synthesis approaches have

21 attempted simultaneous W and N codoping (WN-codoping) of TiO_2 leading to substantial band gap

22 narrowing.[25–30] However, these studies showed mainly interstitial type of N-doping and the presence

23 of other contaminants such as amino groups and carbonaceous species (inherent to precursors used

24 in chemical methods). So far, the observed increase in EPC activity was mainly associated with the

1 effective bandgap reduction and surface area increase[25,28,31] with almost no focus and/or

2 optimisation of the electronic passivation induced by the co-doping approach. This calls for a more

3 systematic experimental study of the structural, electronic, and chemical effects resulting from W

4 and N codoping of TiO_2, over the largest dopant range accessible. The objective being to achieve

5 substitutional doping and identify the optimal doping concentrations leading to both narrowest

6 bandgap and a minimum of photocharges trapping and/or recombination (i.e. longer lifetimes of the

7 photogenerated charges). Practically, an effective co-doping of the TiO_2:WN photoanodes will

8 translate into higher EPC photocurrent, which in turn will degrade more efficiently a given

9 contaminant in water.

10 In this paper, we report on the *in-situ* co-doping of TiO_2 films by both W and N atoms by using a

11 reactive magnetron-sputtering process. By concomitantly adjusting the N_2-to-Ar gas flow ratio and

12 the W-to-TiO_2 target power ratio in the RF-sputtering plasma source, we were able to control the W

13 and N incorporation rates into the films, over the (0 - 3) at.% and (0 - 9) at.% concentration ranges,

14 respectively. The effects of both mono-doping (N and W taken separately), and WN-codoping

15 approaches on the structural, optical, and chemical properties of the sputtered TiO_2 films have been

16 systematically investigated. By achieving detailed experimental analyses of the energy band

17 structure of the doped TiO_2 films, we have recently demonstrated that optimal W and N doping

18 contents correspond not only to the narrowest E_g value of ~2.2 eV, but also to favorable Fermi level

19 (E_F), CBM, and VBM band positions.[32] In the present paper, the codoped TiO_2:WN films are shown

20 to not only possess favorable optoelectronic properties but most interestingly to exhibit also densities

21 of oxygen vacancies and photocharge recombination centers lower than in their mono-doped

22 counterparts, confirming thereby the achievement of an electronically passivated acceptor-donor co-

23 doping approach. To assess the practical advantages of such a co-doping approach, the optimised

24 TiO_2:WN films were integrated into photo-anodes for the EPC degradation of atrazine (a pesticide,

1 and residual contaminant in water) under simulated AM1.5 solar light, and found to deliver superior

2 EPC performance their mono-doped photoanode counterparts.

3

4 **Experimental**

5 All the films were deposited from the sputtering of a TiO_2 target by using an RF (13.56 MHz)

6 magnetron gun operating at a constant power density of 8.8 W/cm^2. The *in-situ* N-doping of the

7 films was achieved through the introduction of N_2 in conjunction with the Ar sputtering gas, whereas

8 W-doping was obtained through the co-sputtering of both TiO_2 and W targets (3"-diam. and 99.99%

9 purity). For the WN-codoping, both N_2 gas and W target co-sputtering were combined with the main

10 TiO_2 target sputtering. Prior to deposition, the chamber was cryopumped to a base pressure of 2 ×

11 10^{-8} Torr. Thereafter, high purity Ar (99.999 %) and N_2 (99.995 %) gases were introduced into the

12 deposition chamber. High purity O_2 (99.995%) was also used for the deposition of the reference

13 TiO_2. The gas flow rates were monitored to maintain a constant pressure of 1.4 mTorr inside the

14 chamber during the sputter-deposition process. In order to control the N incorporation in the

15 TiO_2:WN and TiO_2:N films, the relative nitrogen mass flow rate ratio R_{N2} (i.e. $[N_2]/([N_2]+[Ar])$ was

16 varied between 0 and 15%. The W incorporation was controlled by varying the W target power

17 density (W_{power}) from 50 mW/cm^2 to 250 mW/cm^2. The TiO_2:WN films were simultaneously

18 deposited onto different substrates, including: (i) undoped and double side-polished Si(100), (ii)

19 quartz, and (iii) deployed (10 cm x 11 cm) Ti-grids. The substrates were mounted on a holder located

20 off-axis at a distance of 20 cm from the target, and heated during deposition by a quartz lamp heater

21 to an actual on-substrate temperature of ~470 °C. Prior to film deposition, the target was

22 systematically sputter-cleaned with Ar ions for ~15 min with the shutters closed. The thickness of

23 the TiO_2:WN films was *in-situ* monitored by means of a calibrated quartz-crystal microbalance and

24 *ex-situ* measured through cross-section scanning electron microscopy (SEM) observations by means

of a Jeol JSM-6300F SEM system. No post-acceleration voltage was intentionally applied to the substrates during the sputter-deposition process (they were nonetheless subjected to a built-in plasma sheath bias of ~ -14 V during their growth). The atomic composition and chemical bonding states of the films were systematically investigated by means of X-ray photoelectron spectroscopy (XPS). The XPS spectra were collected by using the ESCALAB 220i-XL spectrophotometer, equipped with an Al$K\alpha$ (1486.6 eV) twin-anode source, after a systematic *in-situ* surface cleaning by means of 5 keV Ar$^+$ ion sputtering gun. The crystalline structure of the films on quartz substrates was characterized by means of a PANalytical X-Pert Pro X-ray diffractometer (XRD) system using Cu$K\alpha$ radiation of 1.5418 Å. The ultra-violet and visible (UV-Vis) transmittance and reflectance spectra of the TiO$_2$:WN films were systematically measured by using an Agilent/Varian Cary 5000 system. Thus, their E$_g$ values were derived from UV-Vis Tauc plot extrapolation. The EPC properties of the TiO$_2$:WN films deposited onto deployed titanium-grid substrates (used as photoanodes) were evaluated in an EPC reactor of which details are described elsewhere[33].

Results and Discussion

The structural and morphological features arising from the concomitant incorporation of N and W atoms into TiO$_2$ were studied via cross-section SEM observations. We have previously showed that the introduction of N$_2$ in the deposition chamber leads to an energetic competition between the the dissociation of N$_2$ molecules and the production ions that contribute to the sputtering process itself.[7] Here, we focus on the concomitant interplay between W and N sources and their effects on the deposited films. Figure 1(a) presents the deposition rate as a function of W$_{power}$ (bottom x-axis; with R$_{N2}$ kept constant at 6%), and R$_{N2}$ (top x-axis; with W$_{power}$ kept constant at 132 mW/cm^2). We note that N$_2$ introduction creates a competitive balance between the energy consumption for N$_2$ molecule dissociation and sputtering ion production with an optimal deposition point at around 7% R$_{N2}$. It is

1 expected that this optimal point should shift to higher R_{N2} as more power is put in the system.

2 Additionally, we note that increasing the power imposed on the W target while maintaining R_{N2}

3 constant linearly increased the deposition rate. This power dependence of the deposition rate is

4 typical for metallic targets in a sputtering process.[34] The morphology of the sputter-deposited

5 TiO_2:WN films showed no significant differences as a function of deposition parameters. From that

6 perspective, all the sputter-deposited films were found to be dense, smooth, and exhibit a uniform

7 apparent morphology regardless of W_{power} or R_{N2}. A typical cross sectional SEM image of a

8 TiO_2:WN film can be seen in Figure 1(b), the deposition parameters for this film were the crossover

9 point from Figure 1(a): W_{power} = 132 mW/cm^2 and R_{N2} = 6%. The thicknesses of the films

10 investigated here are in the 200-400 nm range, depending on the deposition conditions. The exact

11 film thickness will be used for each corresponding film for the determination of its optical absorption

12 coefficient.

13 The effectiveness of our sputter process to incorporate N and W dopants in the TiO_2:WN films was

14 investigated by means of XPS analysis of the N $1s$, Ti $2p$, O $1s$, W $4f$, and W $4p$ core level spectra.

15 The variation of deposition parameters W_{power} and R_{N2} on the incorporation of each dopant is

16 presented in Figure 2. Figure 2(a) shows the incorporation of W (left y-axis) and N (right y-axis)

17 atoms with varying R_{N2} while W_{power} is maintained constant at 132 mW/cm^2. From this Figure 2(a),

18 one can see that the increase of R_{N2} translates into a progressive increase of N incorporation.

19 However, it is also seen that the increase of N incorporation occurs to the detriment of W

20 incorporation. The increase of N content with R_{N2} is a direct consequence of an increased amount

21 of N atoms in the plasma mix during the deposition process. This results into more N atoms available

22 for incorporation, which enter in a sort of competition with W atoms (at a fixed power on the W

23 target), lowering thereby their incorporation when R_{N2} is increased. In contrast, when the R_{N2} is

1 fixed (at 6% here) and W_{power} is increased, the incorporation of both N and W steadily increase with

2 W_{power}, as shown in Figure 2(b). This behavior can be explained by two facts: (i) the incorporation

3 of W into the TiO_2 lattice is expected to increase the solubility limit of the N dopant.[5,23] The

4 solubility increase is caused mainly by the introduction of W atoms into the TiO_2 lattice which

5 lowers the formation energy of substitutional N and increases the total free valence of the

6 matrix.[21,23,24] Secondly, (ii) the increase of W_{power}, while keeping a constant R_{N2}, leads to more

7 sputtered W atoms and concomitantly provides additional energy for the dissociation of N_2

8 molecules into N atoms. Figures 2 (a) and (b) highlight the ability of our process to precisely control

9 the incorporation levels of each dopant in the sputtered TiO_2 films through the appropriate tuning of

10 both W_{power} and R_{N2}. Finally, the fundamental characteristics of the XPS binding energy (BE) spectra

11 were found to be very similar within the investigated concentration ranges (i.e. 0 to ~3 at.% and 0

12 to ~9 at.% for W and N contents, respectively). Indicating that for these doping levels, the chemical

13 bonding of these films may vary in content (depending on the doping levels), but their nature remains

14 the same.

15 Figure 3 shows the high-resolution BE spectra of the O *1s*, Ti *2p*, N *1s*, and W *4f* (from left to right

16 respectively) core levels for different films, namely TiO_2, TiO_2:N, TiO_2:W, and TiO_2:WN films

17 (from bottom to top, respectively). These core level spectra were deconvoluted into their different

18 components corresponding to various local electronic environments (oxidation/bonding states). For

19 the TiO_2 films, the Ti $2p_{3/2}$ peak can be decomposed into two main components corresponding to

20 two oxidation states of Ti, namely Ti[IV] and Ti[III] at 458.6 eV and 456.9 eV, respectively, with their

21 corresponding Ti $2p_{1/2}$ energy levels found at 5.7 eV and 5.5 eV higher BE, having 1:2 branching

22 ratios.[7,31,35–37] For subsequent W *4f* fitting purposes (as the Ti *3p* energy window overlaps the W *4f*

23 peak energies), Ti *3p* peaks were deconvoluted to reveal Ti[IV] and Ti[III] oxidation state peaks at 37.1

1 eV and 35.7 eV respectively,[38,39] in full agreement with the Ti *2p* derived quantifications. The

2 presence of Ti^{III} can be attributed to sub-stoichiometric species formed mainly as a result of

3 preferential sputtering during thin film deposition.[7,40] Given that Ar^+ ion etch-cleaning is used to

4 eliminate surface carbonaceous contaminants prior to acquisition, the Ti^{III} quantification is assumed

5 to be slightly overestimated. However, this contribution is expected to remain unchanged for all

6 surveyed samples as surface etch-cleaning parameters were kept constant.[7,36,40] This feature is

7 important as its presence is indicative of V_O in the lattice, a defect associated with high levels of

8 photocharge recombination.[4,8,41] The Ti *2p* states can be inferred in the corresponding O *1s* core

9 levels. The main $O^{(TiIV)}$ peak at 529.9 eV is associated with lattice oxygen in the TiO_2 matrix; we

10 note that sub-stoichiometric lattice oxygen can also be distinguished and identified as $O^{(TiIII)}$ at

11 ~0.5eV higher binding energy.[35,36] Additionally, we note the presence of a third peak, denoted as

12 $O^{(H)}$ at 530.7 eV and about double the FWHM of the other O *1s* peaks. Commonly, this peak is

13 attributed to O *1s* defective oxygen and surface hydroxide species.[35,36,42] This contribution is

14 expected to remain of similar relative intensity in relation to the main O *1s* peaks for all films.[35,36]

15 The XPS derived composition of undoped films, calculated from relative peak intensities, is found

16 to be ~$TiO_{1.87}$.

17 As nitrogen gas is introduced into the deposition chamber (TiO_2:N films), the appearance of the N

18 *1s* peak in the film's XPS spectra can be observed with two characteristic components: N^{sub} and

19 N^{inter} at 396.2 eV and 397.2 eV binding energies, respectively. The N^{sub} peak is known to arise from

20 substitutional -Ti-N- type bonds and the N^{inter} peak is associated with interstitial -O-N type bonds

21 within the titania crystal structure.[4,6,7,11–13] The relative intensity of the peaks confirms that most of

22 the doping is of the substitutional type, associated with the visible light photosensitisation of TiO_2:N

23 via the introduction of N *2p* levels just above the O *2p* composed VBM.[4,6,7,11–13] However, the

1   introduction of N into the thin films is accompanied with the appearance of Ti^{II} oxidation state

2   species in the Ti $2p$ BE spectra (Ti^{II} $2p_{3/2}$ at 455.3 eV and the $2p_{1/2}$ component at 5.6 eV higher BE)

3   and Ti $3p$ (Ti^{II} $3p$ at 34.8 eV).[4,43] This reduced state can also be inferred on the O $1s$ spectra with

4   the appearance of $O^{(TiII)}$ (~1eV higher BE than the $O^{(TiIV)}$ peak).[35,38] These reduced valence states

5   are known to arise from the electronic distortions induced by nitrogen doping, reducing Ti^{IV} species

6   into Ti^{III}, and on a much lesser extent into Ti^{II}. These bonding states are indicative of the lattice

7   compensating for localised deep charge defects (known to arise from interstitial type N doping),

8   mainly via the formation of V_O.[4,7,8,14,41] If substitutional type of doping is considered, the obtained

9   stoichiometry of the N-doped films is $\sim TiO_{1.69}{:}N_{0.12}$ (total N ~6.3 at.%, with N_{sub} ~4.2 at.%); this

10   relatively low O content indicates a high density of V_O present within the thin films, justifying the

11   significant increase of highly reduced Ti species.

12   The addition of tungsten (W) in the co-sputtering process, via sputtering of a metallic W target

13   concomitantly with the TiO_2 target sputtering, leads to the appearance of two main features in the

14   W $4f$ BE window of the $TiO_2{:}W$ thin-films (Figure 3). These W $4f$ peaks are due to the W^{VI} and W^{IV}

15   states in the oxide form with the main $4f_{7/2}$ components appearing at 34.5 eV and 32.3 eV,

16   respectively, with the corresponding $4f_{5/2}$ doublets found at 2.2eV higher BE with a 3:4 peak

17   intensity ratio.[37,44–47] The appearance of the $O^{(W)}$ peak at 529.2 eV in the O $1s$ spectra can be inferred,

18   as some of oxygen species are associated with W.[46] The XPS derived composition of these films is

19    $\sim TiO_{1.84}{:}W_{0.06}$ (total W ~2.3 at.%). From these analyses, we note that W doped films present lower

20   density of V_O than N doped films. This aligns with theoretical models predicting that W-doping

21   should reduce the formation of V_O (increase in formation energy) as compared to N-doping.[20]

22   Due to size constraints, W and N are mostly expected to substitute for Ti and O atoms, respectively

23   (nonetheless, interstitial N is also possible as above discussed), and -W-N- type bonds are

1   energetically superimposed to -Ti-N- type bonds.[48,49] Therefore, little effect is expected in the N $1s$

2   and corresponding cation signatures. Thus, it can be confirmed that both the W and N species are

3   incorporated into mostly substitutional locations within the TiO_2 matrix as they present identical

4   chemical energy states as the TiO_2:N[4,6,7] and TiO_2:W.[37,44–46] This being said, the XPS derived

5   composition of this codoped film is ~$TiO_{1.83}$:$W_{0.04}N_{0.09}$ (N ~4.9 at.% and W ~1.2 at.%). This film

6   composition indicates that there is a lack of O in the films, at a similar atomic proportions as in the

7   undoped samples (which were interestingly deposited with additional oxygen during sputtering).

8   This indicates that there are less oxygen vacancies in the codoped films as compared to the N-

9   monodoped ones. This is in accordance with theoretical models that predict that when both dopants

10 (W and N) are introduced simultaneously, there is a significant reduction of electronic defect

11 formation (such as V_O).[5,18–21,23,24] Table 1 summarises the XPS derived dopant levels of the

12 TiO_2:WN films along with their corresponding thickness, as determined from SEM cross-section

13 observations.

N (at.%)	W (at.%)	Thickness (nm)
0.0	0.0	200
2.4	0.0	260
5.7	0.0	250
0.0	0.6	400
0.0	2.3	380
0.0	3.1	430
2.5	2.4	300
5.9	0.7	310
6.4	1.1	300
7.2	1.6	300
8.9	2.4	410
4.9	1.2	370
8.5	0.9	270
7.7	0.2	270
7.9	0.3	280
8.7	3.6	340
6.4	3.6	270

1 Table 1: Film thickness (as derived from SEM observations) and total dopant contents (from XPS) for the samples used in the UV-Vis. characterizations.

2

3 Our previous work has shown that the N substitutional doping significantly affects the optical

4 properties of the N-doped TiO_2 films, namely narrowing their bandgap.[7] Hence, the effect of W and

5 N dual doping on the optical properties of the TiO_2:WN films was systematically investigated as a

6 function of the doping scheme (i.e., N, W, and WN). Figure 4(a) shows UV-Vis transmittance

7 spectra of the $TiO_{1.87}$, $TiO_{1.84}$:$W_{0.06}$, $TiO_{1.69}$:$N_{0.12}$, and $TiO_{1.83}$:$W_{0.04}N_{0.09}$ films deposited onto quartz

8 substrates. We note a significant red shift of the absorption band edge of the spectra from about

9 320nm for undoped TiO_2 films to ~420nm for the $TiO_{1.69}$:$N_{0.12}$ films, and to ~440 nm for

10 $TiO_{1.83}$:$W_{0.04}N_{0.09}$ films. In agreement with our previous work, our results showed that any doping

11 content beyond this doping point did not necessarily translate into further red shifting of the

12 absorption edge.[7] It is to be noted that the W-doped films ($TiO_{1.84}$:$W_{0.06}$) showed the same absorption

13 edge as undoped TiO_2 films (no red-shift). This confirms that it is indeed nitrogen that produces

14 energy states responsible for the observed photosensitization of the TiO_2:WN films in the visible. In

15 order to derive a quantitative value of the E_g for these thin films, the corresponding UV-Vis spectra

16 (transmittance and reflectance used to extract the absorption coefficient) were analyzed according

17 to the Tauc formalism,[45] where the E_g value can be deduced from the x-intercept of the tangential

18 extrapolation of the Tauc plots, as shown in Figure 4(b). We note that indeed, both the $TiO_{1.69}$:$N_{0.12}$,

19 and $TiO_{1.83}$:$W_{0.04}N_{0.09}$ samples show significant optical E_g reduction to around ~2.3 eV, while the

20 $TiO_{1.87}$ and $TiO_{1.84}$:$W_{0.06}$ films exhibit an E_g of ~3.2 eV, consistent with indirect gap values quoted

21 for titania in the literature.[4,8] These results confirm that W doping has no significant impact on the

22 absorption edge of the films, while the N doping induced visible photosensitisation is still effective

23 in the co-doping scheme. In order to get a broader picture, the E_g values were derived for numerous

24 TiO_2:WN codoped films with a broader range of doping levels and reported in a sort of a 2D map

of which X and Y axes are N and W doping level, as shown in Figure 5. We note that in the Y-axis

(W concentration) that there is a very little to no effect on the E_g variation (varying W by about 3

at.% induces only a small ~0.2 eV change in E_g value), mostly through the creation of shallow states

below the CB.[19,50] In contrast, the main determining factor for bandgap narrowing of the TiO_2:WN

films (and thereby their photosensitisation to visible light) is their N doping level. Additionally, we

noticed that beyond a N-doping level ~6 at.% of N, no additional gain in visible light absorption can

be obtained. This points up the existence of an optimal nitrogen doping concentration range (5-6

at.%) where the E_g stays at its lowest value of ~2.3 eV (a bandgap value that ensures effective visible

light photosensitization of TiO_2 films). This observation, along with the theoretical prediction[20] that

states that the acceptor-donor passivation is most efficient with the N:W ratio close to 2:1 is what

guided the selection of our representative TiO_2:WN samples to be used for further analysis. Thus,

the following film compositions were investigated: $TiO_{1.87}$, $TiO_{1.84}$:$W_{0.06}$, $TiO_{1.69}$:$N_{0.12}$, and

$TiO_{1.83}$:$W_{0.04}N_{0.09}$. In order to better understand the relationship between EPC performance and

dopant induced band-gap narrowing, one has to have access to other physical parameters, such as

the Fermi energy, work function, and valence band maximum (VBM)/conduction band minimum

(CBM) energy levels (a study that is beyond the scope of the present paper). In fact, the measurement

and quantification of the above-mentioned optoelectronic characteristics of the doped TiO_2 films in

order to reconstruct the band energy diagrams is a thorough study that has been reported elsewhere.[32]

We briefly highlight here some of the relevant insights gained from this study[32] : first, (i) W-doping

keeps most of the E_g features unchanged outside of the introduction of new states below the CBM,

(ii) N-doping shrinks the E_g mostly via the introduction of new mid-gap N *2p* states above the mostly

O *2p* populated VBM while reducing the work function, and (iii) WN-codoping shrinks the E_g

mostly via hybridizing N *2p* states with VBM O *2p* states while leaving most other features

unchanged.[32] In summary, while both N-doped and WN-codoped samples show a significant

1   reduction in their E_g, the acceptor-donor codoped samples are expected to outperform monodoped

2   ones due to less midgap states, defect states, and better placements of the VBM energy levels.[32]

3   It is worth reiterating that the crystallinity of the films plays a key role in their EPC properties as it

4   determines features such as the bandgap, average crystallite size (mean free path of charges), etc[4,8].

5   Therefore, we have used XRD to investigate the crystalline structure of our films as a function of

6   their doping scheme, and the obtained spectra are displayed in Figure 6. The $TiO_{1.87}$ films are seen

7   to crystallize in the anatase (A) phase with the characteristic (101), (103), (004), (112), (200), (105),

8   and (211) peaks (JCPDS no.: 84-1286); with the main A(101) peak at 25.4° with 0.4° of full width

9   at half maximum (FWHM). The Williamson-Hall size-strain analysis[51] revealed lattice parameters

10 typical of anatase under low tensile strain (~0.66%), as shown in Table 2. This is most likely due to

11 the oxygen vacancies present in the structure, causing some of the Ti atoms to reduce from Ti^{IV} to

12 Ti^{III} (as above-shown by XPS), increasing their atomic radii. When nitrogen is incorporated into the

13 structure, the crystalline quality of the TiO_2:N films is significantly reduced as seen in Figure 6

14 (signal to noise ratio and FWHM ~0.7° for the A(101)). The tensile strain of the TiO_2:N films

15 increased to ~2.75%, explaining the observed relative deterioration of their crystalline quality. This

16 strain exists due to a couple of reasons: (i) N-doping reduces the formation energy of V_O facilitating

17 sub-stoichiometric oxide formation,[4,23,24,52,53] and (ii) interstitial N-doping will impose a certain

18 stretching of the lattice.[54] In the case of W doping, the crystallinity of the TiO_2:W films is also seen

19 to be greatly affected. Given that W^{VI} and Ti^{IV} are of similar ionic radii (around 0.600 Å and 0.605

20 Å), substitutional W^{VI} doping should not affect the TiO_2 lattice structure significantly. However, as

21 shown by XPS analysis in Figure 3 we note the presence of W^{IV} species in the TiO_2 structure, this

22 reduced state is of higher atomic radii (0.660 Å) and is associated with the distortion of the crystal

23 lattice to higher 2θ values.[37] Additionally, W^{IV} species (WO_2 type crystal) naturally crystallize in a

1 rutile structure.[55] In fact, this and the W doping generated strain (as high as ~4.06%) in the lattice

2 induce the TiO_2:W films to transition into the rutile polymorph.[7,37] In Figure 6 the rutile phase peaks

3 are seen to be predominant and very broad (with a FWHM as large as ~2.1° for the R(110) peak).

4 The less intense anatase peak (A(101) is also found to be very broad with a FWHM of ~1.9°).

5 Interestingly, in the case of WN-codoping, the anatase phase is recovered with a high crystalline

6 quality (the FWHM of the anatase (101) peak FWHM is of ~0.5°) and a moderate tensile strain

7 (estimated to ~1.9%). The crystallite size (of ~30 nm) of these codoped films was found to be very

8 comparable to that of undoped $TiO_{1.87}$ films. Moreover, one can note that the strain in the WN-

9 codoped films is lower as compared to their monodoped counterparts (i.e. W-doped and N-doped;

10 see Table 2). This recovery of the anatase phase seems to be a direct result of local dopant charge

11 passivation, leading to a reduction of structural defects that arise from uncompensated lattice

12 charges. Indeed, substitutional W and N dopants have been reported to result in a charge-passivated

13 lattice with lower V_O formation.[21-24]

Sample	TiO_2	$TiO_{1.89}$	$TiO_{1.84}$:$W_{0.06}$	$TiO_{1.69}$:$N_{0.12}$	$TiO_{1.83}$:$W_{0.04}N_{0.09}$
a (nm)	0.378	0.378	N/A	0.381	0.384
b (nm)	0.378	0.378	N/A	0.381	0.384
c (nm)	0.950	0.944	N/A	0.966	0.934
c/a	0.251	0.250	N/A	0.254	0.243
Vol. (nm^3)	0.136	0.135	N/A	0.140	0.138
Crys. Size (nm)	N/A	27.68	6.40	7.00	32.93
Internal strain (η)	0.00%	0.66%	4.10%	2.75%	1.90%

14 Table 2: Williamson-Hall calculated lattice parameters based on the XRD spectra of Figure 4 for

15 the various doping schemes alongside theoretical TiO_2 lattice values.

16 Finally, in order to assess the electro-photocatalytic properties of our doped TiO_2 films, while taking

17 advantage of their visible light photosensitisation and the acceptor-donor passivated codopants, the

18 codoped $TiO_{1.83}$:$W_{0.04}N_{0.09}$ films along with $TiO_{1.87}$, $TiO_{1.69}$:$N_{0.12}$, and $TiO_{1.84}$:$W_{0.06}$ films were

1   deposited onto both sides of deployed Ti-grid substrates (10 cm x 11 cm) and used as photoanodes.

2   Those photoanodes were integrated into a home built electro-photocatalytic (EPC) reactor (of which

3   details can be found elsewhere[33]). The EPC performance of our photoanodes was assessed towards

4   the degradation of a real emerging contaminant that is atrazine. Atrazine is a pollutant that is widely

5   used as a pesticide in agriculture. For the purpose of the present study, synthetic solutions containing

6   atrazine concentrations of 60 $\mu g/L$ (60 ppb, as these are the typical concentrations of heavily polluted

7   areas) were prepared and treated in our EPC reactor under AM 1.5G solar simulator while

8   continuously circulating the solution during the treatment time which was of up to 2 hours. The

9   reaction kinetics for the four different types of photoanodes are shown in Figure 7(a). We note that

10   while $TiO_{1.87}$ is found to degrade atrazine, the degradation reaction is relatively slow (after 1 hour

11   of treatment, ~20 ppb of atrazine I still present in the solution). In the case of $TiO_{1.69}:N_{0.12}$

12   photoanodes, the degradation efficiency is seen to improve due to the photosensitisation effect of

13   nitrogen doping; allowing the use of a higher portion of visible light photons for the generation of

14   excitons to be used in the photocatalytic process.[7,33] Surprisingly, $TiO_{1.84}:W_{0.06}$ photoanodes were

15   found to perform similarly (within the statistical error margin) to the photosensitized $TiO_{1.69}:N_{0.12}$,

16   even if their bandgap is much larger than that of N-doped TiO_2. This effect is mainly attributed to

17   the W induced increase of the photocharge lifetimes of the $TiO_2:W$ films, as compared to the N-

18   doped photoanodes.[19,50,56] In fact, a more systematic study of the effect of the doping scheme on the

19   photocharge lifetimes has been carried out and reported elsewhere.[56] Important to underline here is

20   that the W dopant was found to increase the formation energy of V_O defects, and to locally passivate

21   charge disparities when co-introduced with N.[56] These effects have led to WN-codoped samples

22   exhibiting a very good visible-light sensitivity while having photocharge lifetimes up to three times

23   longer than those measured in their N-doped TiO_2 counterparts (photocharge trapping decay

24   constant of 90 ± 7 ns for $TiO_2:WN$ *versus* 30 ± 10 μs for $TiO_2:N$).[56] This corroborates well with the

1   fact that the codoped TiO$_2$:WN photoanodes are the most effective ones for atrazine degradation, as

2   can be clearly seen in Figure 7(b). Indeed, after just 30 min of treatment, the TiO$_2$:WN photoanodes

3   degraded 94% of the atrazine present in the solution (this represents 24% and 71% more than the N-

4   doped and the undoped TiO$_2$ photoanodes, respectively). Those results clearly confirm the benefit

5   of the TiO$_2$ photoanode WN-codoping for the EPC degradation of pollutants. In fact, nitrogen

6   doping allows for photosensitivity of the photoanodes in the visible domain, permitting thereby the

7   additional use of visible light photons for photocatalysis. However, part of this advantage is

8   counteracted by N doping induced deep states in the E_g that act as recombination centers trapping

9   the photogenerated charges. This drawback, in turn, can be minimised via the electronically

10   passivated WN-codoping approach, allowing for the recovery of a significant increase in EPC

11   performance,[21,23,24] as exhibited here by our TiO$_2$:WN photoanodes.

12   **Conclusion**

13   In summary, we were able to develop and apply a reliable RF magnetron sputtering process for the

14   fabrication on in-situ doped and codoped TiO$_2$ films with different W and N doping concentrations,

15   in the ranging 0-3 at.% and 0-9 at.% ranges, respectively. All the deposited films have shown a

16   dense, smooth, and uniform apparent morphology, regardless of their doping conditions. By

17   adjusting the relevant operating parameters, namely W_{power} and R_{N2}, we were able to fine-tune the

18   incorporation of W and N dopants into the TiO$_2$ films. The XPS analyses have revealed that both

19   the W and N species are mostly incorporated into substitutional doping locations in the TiO$_2$ matrix.

20   The N-doping was shown to increase significantly the density of V_O defects (TiO$_{1.69}$:N$_{0.12}$

21   composition as compared to the undoped TiO$_{1.87}$). In contrast, the (WN) codoping was found to

22   minimise the formation of V_O (i.e.; TiO$_{1.83}$:W$_{0.04}$N$_{0.09}$). From optoelectronic viewpoint, both N-

23   doping and WN-codoping were found to induce a significant red shift of the absorption edge, leading

to a bandgap narrowing by ~0.9 eV. Thus, the bandgap of both TiO_2:N and TiO_2:WN films was found to be in the visible range with a value as low as 2.3 eV. N-doping was pinpointed as the most determining factor for bandgap narrowing. An N-doping concentration of ~5.5 at.% was identified as the optimal content for the narrowest bandgap. Higher N-doping contents do not translate into additional narrowing of the bandap. On the other hand, XRD results have shown a significant decrease in crystalline quality of the films and an increase in their lattice strain in the case of monodoping. This was particularly observed in the case of W-doped films, where the relatively strong tensile strain has led to a transition from anatase to rutile phase. This drawback of monodoping was significantly reduced when the codoping scheme was adopted, as the lattice strain was found to diminish significantly along with the recovery of high crystallinity (of the anatase phase) of the codoped films. Finally, our EPC experiments have shown that TiO_2:WN codoped photoanodes are the most effective for atrazine degradation (93% of atrazine was degraded within the first 30 min of treatment time under AM1.5G solar radiation). Indeed, the codoped TiO_2:WN photoanodes have performed 71% better than the undoped-TiO_2 and 24% better than the N-doped TiO_2:N ones, during the first 30 min of treatment. This emphasizes the benefit of using WN-codoped TiO_2 for EPC applications through the enhanced harvesting of visible light (as evidenced by improved EPC performance) in comparison to N-doped photoanodes. The developed TiO_2:WN photoanodes definitely open up new prospects for the degradation of emerging contaminants in water while using the direct sunlight radiation.

Acknowledgements

References

[1] A. FUJISHIMA and K. HONDA, Nature **238**, 37 (1972).

[2] B. O'Regan and M. Grätzel, Nature **353**, 737 (1991).

[3] S.U.M. Khan, M. Al-Shahry, and W.B. Ingler, Science **297**, 2243 (2002).

[4] A. V. Emeline, V.N. Kuznetsov, V.K. Rybchuk, and N. Serpone, Int. J. Photoenergy **2008**, 1 (2008).

[5] I.S. Cho, C.H. Lee, Y. Feng, M. Logar, P.M. Rao, L. Cai, D.R. Kim, R. Sinclair, and X. Zheng, Nat. Commun. **4**, 1723 (2013).

[6] R. Asahi, Science (80-.). **293**, 269 (2001).

[7] N. Delegan, R. Daghrir, P. Drogui, and M.A. El Khakani, J. Appl. Phys. **116**, 153510 (2014).

[8] A. Fujishima, X. Zhang, and D. Tryk, Surf. Sci. Rep. **63**, 515 (2008).

[9] D.O. Scanlon, C.W. Dunnill, J. Buckeridge, S. a Shevlin, A.J. Logsdail, S.M. Woodley, C.R. a Catlow, M.J. Powell, R.G. Palgrave, I.P. Parkin, G.W. Watson, T.W. Keal, P. Sherwood, A. Walsh, and A. a Sokol, Nat. Mater. **12**, 798 (2013).

[10] C. Di Valentin, G. Pacchioni, A. Selloni, S. Livraghi, and E. Giamello, J. Phys. Chem. B **109**, 11414 (2005).

[11] C. Di Valentin, G. Pacchioni, and A. Selloni, Phys. Rev. B **70**, 85116 (2004).

[12] J. Lynch, C. Giannini, J.K. Cooper, A. Loiudice, I.D. Sharp, and R. Buonsanti, J. Phys. Chem. C **119**, 7443 (2015).

[13] F. Peng, L. Cai, H. Yu, H. Wang, and J. Yang, J. Solid State Chem. **181**, 130 (2008).

[14] G.R. Torres, T. Lindgren, J. Lu, C.-G. Granqvist, and S.-E. Lindquist, J. Phys. Chem. B **108**,

, 5995 (2004).

[15] M. D'Arienzo, N. Siedl, A. Sternig, R. Scotti, F. Morazzoni, J. Bernardi, and O. Diwald, J. Phys. Chem. C **114**, 18067 (2010).

[16] B. Liu, L. Wen, and X. Zhao, Mater. Chem. Phys. **106**, 350 (2007).

[17] R. Katoh, A. Furube, K. Yamanaka, and T. Morikawa, J. Phys. Chem. Lett. **1**, 3261 (2010).

[18] W.-J. Yin, H. Tang, S.-H. Wei, M.M. Al-Jassim, J. Turner, and Y. Yan, Phys. Rev. B **82**, 45106 (2010).

[19] V. Çelik and E. Mete, Phys. Rev. B **86**, 205112 (2012).

[20] M. Li, J. Zhang, and Y. Zhang, Chem. Phys. Lett. **527**, 63 (2012).

[21] R. Long and N.J. English, Chem. Mater. **22**, 1616 (2010).

[22] R. Long and N.J. English, Appl. Phys. Lett. **94**, 132102 (2009).

[23] D. Wang, Y. Zou, S. Wen, and D. Fan, Appl. Phys. Lett. **95**, 12106 (2009).

[24] Y. Gai, J. Li, S.-S. Li, J.-B. Xia, and S.-H. Wei, Phys. Rev. Lett. **102**, 36402 (2009).

[25] X. Cui, S. Rong, Y. Cao, Y. Yin, S. Li, and M. Li, Appl. Phys. A **113**, 47 (2013).

[26] S.S. Thind, G. Wu, M. Tian, and A. Chen, Nanotechnology **23**, 475706 (2012).

[27] S.S. Thind, G. Wu, and A. Chen, Appl. Catal. B Environ. **111–112**, 38 (2012).

[28] A. Kubacka, B. Bachiller-Baeza, G. Colón, and M. Fernández-García, Appl. Catal. B Environ. **93**, 274 (2010).

[29] A. Folli, J.Z. Bloh, E.-P. Beukes, R.F. Howe, and D.E. Macphee, J. Phys. Chem. C **117**, 22149 (2013).

[30] J.Z. Bloh, A. Folli, and D.E. Macphee, J. Phys. Chem. C **118**, 21281 (2014).

[31] S.S. Thind, G. Wu, M. Tian, and A. Chen, Nanotechnology **23**, 475706 (2012).

[32] R. Pandiyan, N. Delegan, A. Dirany, P. Drogui, and M.A. El Khakani, J. Phys. Chem. C **120**, 631 (2016).

[33] R. Daghrir, P. Drogui, I. Ka, and M.A. El Khakani, J. Hazard. Mater. **199–200**, 15 (2012).

[34] L.I. Maissel, R. Glang, and P.P. Budenstein, J. Electrochem. Soc. **118**, 114C (1971).

[35] M.C. Biesinger, B.P. Payne, A.P. Grosvenor, L.W.M. Lau, A.R. Gerson, and R.S.C. Smart, Appl. Surf. Sci. **257**, 887 (2010).

[36] M.J. Jackman, A.G. Thomas, and C. Muryn, J. Phys. Chem. C **119**, 13682 (2015).

[37] S. Sathasivam, D.S. Bhachu, Y. Lu, N. Chadwick, S. a. Althabaiti, A.O. Alyoubi, S.N. Basahel, C.J. Carmalt, and I.P. Parkin, Sci. Rep. **5**, 10952 (2015).

[38] F. Werfel and O. Brümmer, Phys. Scr. **28**, 92 (1983).

[39] J. Riga, C. Tenret-Noël, J.J. Pireaux, R. Caudano, J.J. Verbist, and Y. Gobillon, Phys. Scr. **16**, 351 (1977).

[40] D. Brassard, M. a. El Khakani, and L. Ouellet, J. Appl. Phys. **102**, 34106 (2007).

[41] A.K. Rumaiz, J.C. Woicik, E. Cockayne, H.Y. Lin, G.H. Jaffari, and S.I. Shah, Appl. Phys. Lett. **95**, 262111 (2009).

[42] M. Kitano, K. Funatsu, M. Matsuoka, M. Ueshima, and M. Anpo, J. Phys. Chem. B **110**, 25266 (2006).

[43] M.-S. Wong, H. Pang Chou, and T.-S. Yang, Thin Solid Films **494**, 244 (2006).

[44] T. Mishra, M. Mahato, N. Aman, J.N. Patel, and R.K. Sahu, Catal. Sci. Technol. **1**, 609 (2011).

[45] J. Li, J. Xu, W.L. Dai, H. Li, and K. Fan, Appl. Catal. B Environ. **82**, 233 (2008).

[46] K. T. Ng and D.M. Hercules, J. Phys. Chem. **80**, 2094 (1976).

[47] M. Sun, N. Xu, Y.W. Cao, J.N. Yao, and E.G. Wang, J. Mater. Res. **15**, 927 (2000).

[48] Y.-C. Nah, I. Paramasivam, R. Hahn, N.K. Shrestha, and P. Schmuki, Nanotechnology **21**, 105704 (2010).

[49] Y. Zhao, W. Hu, Y. Xia, E. Smith, Y. Zhu, C. Dunnill, and D. Gregory, J. Mater. Chem. (2007).

[50] X.. Li, F.. Li, C.. Yang, and W.. Ge, J. Photochem. Photobiol. A Chem. **141**, 209 (2001).

[51] G.. Williamson and W.. Hall, Acta Metall. **1**, 22 (1953).

[52] A. Kumar and T. Mohanty, J. Phys. Chem. C **118**, 7130 (2014).

[53] L. Wan, J.F. Li, J.Y. Feng, W. Sun, and Z.Q. Mao, Mater. Sci. Eng. B **139**, 216 (2007).

[54] Y. Shen, T. Xiong, T. Li, and K. Yang, Appl. Catal. B Environ. **83**, 177 (2008).

[55] F.J. Wong and S. Ramanathan, J. Mater. Res. **28**, 2555 (2013).

[56] N. Delegan, R. Pandiyan, S. Johnston, A. Dirany, S. Komtchou, P. Drogui, and M.A. El Khakani, J. Phys. Chem. C 7b11266 (2018).

1 **Figures**

2
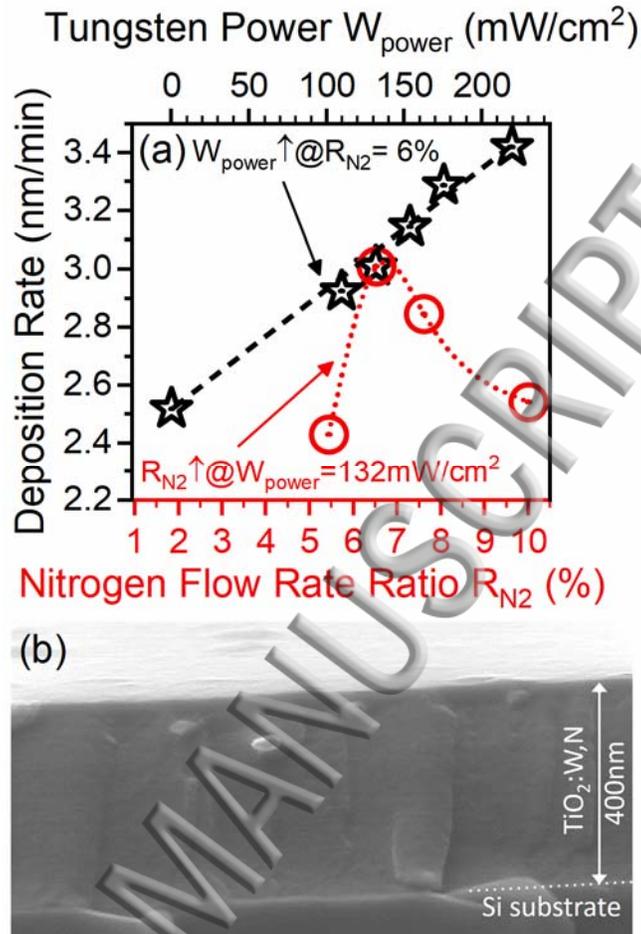
Figure 1: (a) variation of deposition rate at constant R_{N2} (black dash-dot line) with varying W_{power} and the variation with constant W_{power} with varying R_{N2} (red dash line); (b) SEM micrograph of a $W_{power} = 132$ mW/cm^2 and $R_{N2} = 6$ % deposited TiO$_2$:WN film.
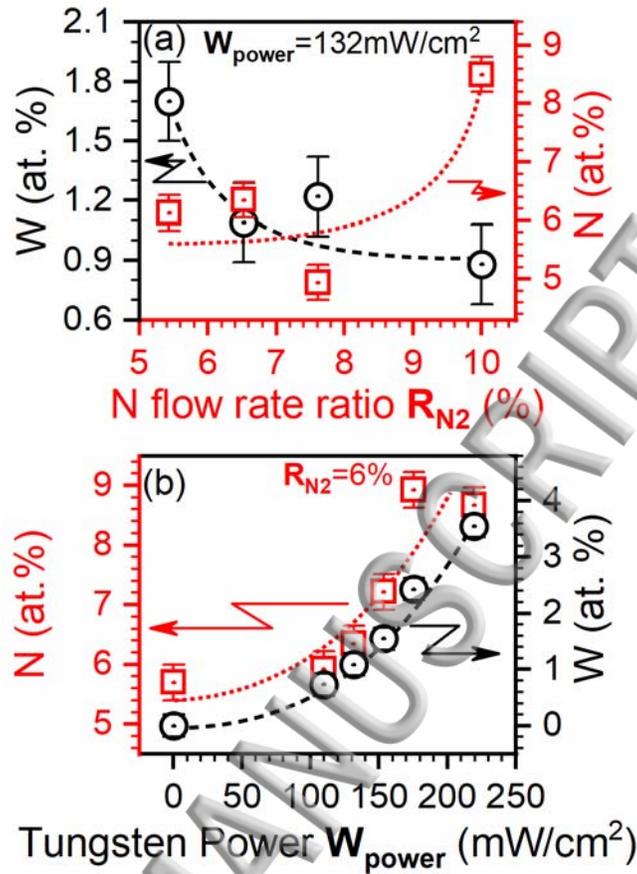
Figure 2: (a) W and N incorporation rate (left and right hand y-axis respectively) at constant W_{power} with varying R_{N2}, (b) N and W incorporation (left and right hand y-axis respectively) at constant R_{N2} with varying W_{power}.
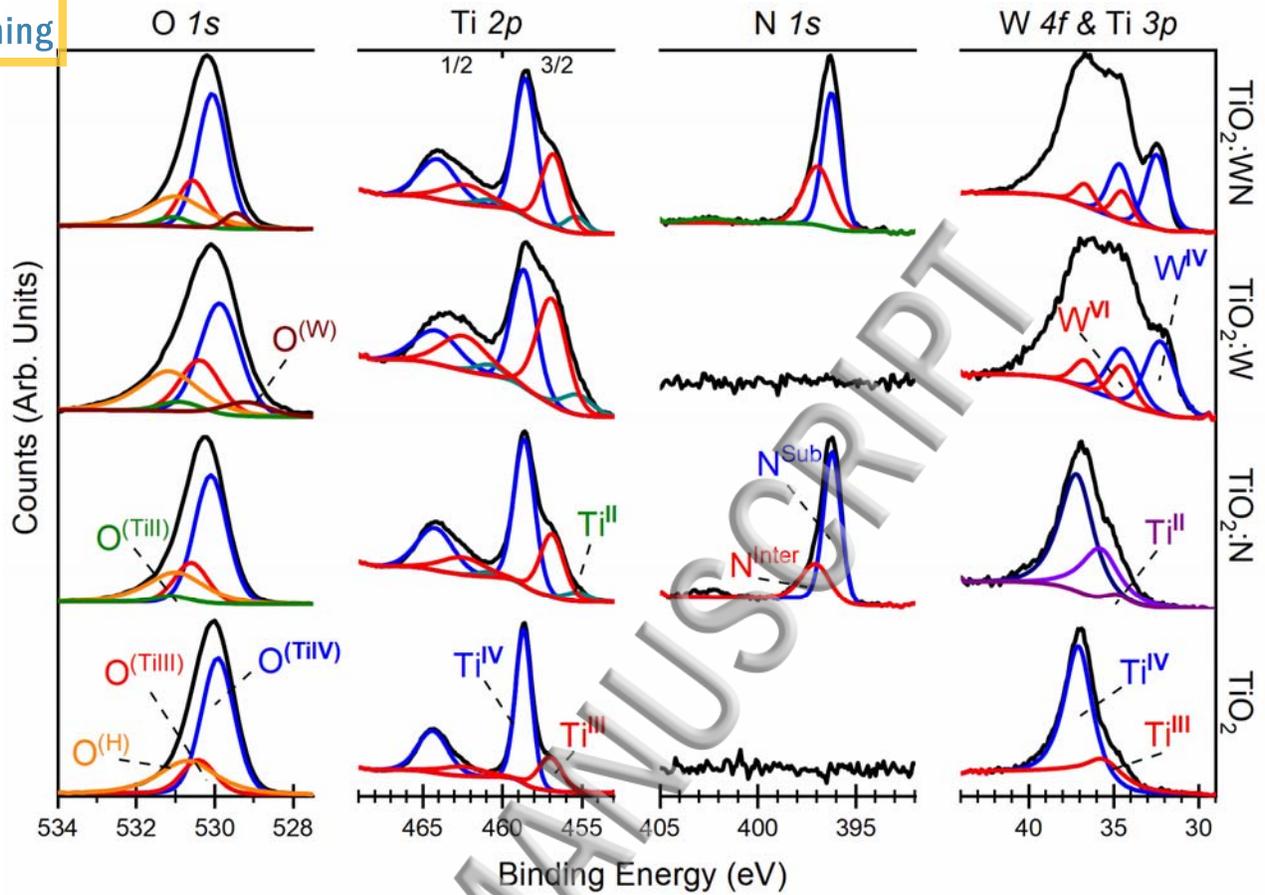
Figure 3: High-resolution XPS spectra of the O 1s (a), Ti 2p (b), N 1s (c), and W 4f core levels (from left-to-right) of the TiO_2, TiO_2:N, TiO_2:W, and TiO_2:WN films (from bottom-to-top) as a function of each doping scheme. Ti 3p signatures obscured in the case of W containing films as to prioritise visibility of W 4f levels.
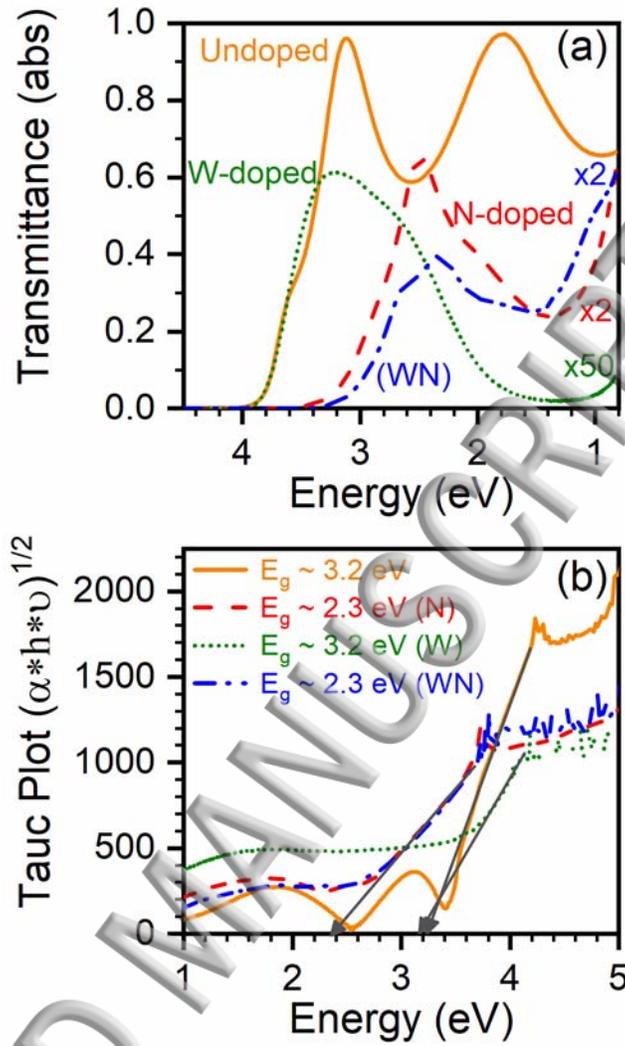
Figure 4: (a) Selected UV-Vis transmittance spectra of the sputter-deposited TiO_2, TiO_2:N, TiO_2:W, and TiO_2:WN films (b) Tauc plots of those films with their corresponding extrapolated E_g values.
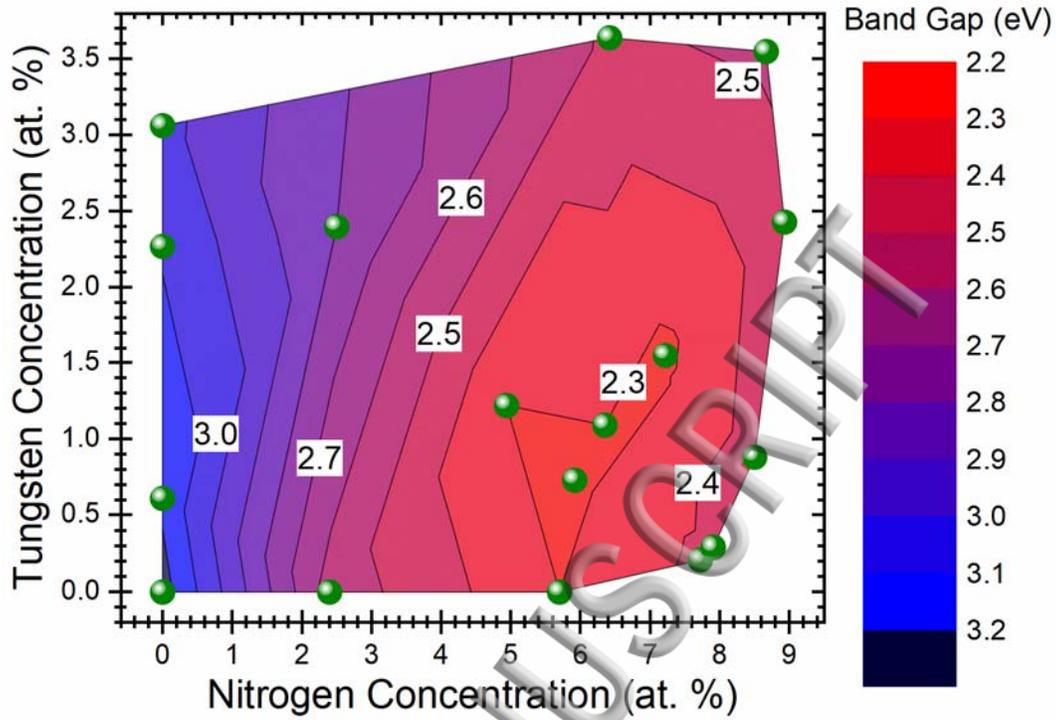
Figure 5: 2D-map displaying the variation of E_g as a function of both Nitrogen and Tungsten doping concentrations. The color scale (on the right-hand side) depicts the bandgap values.
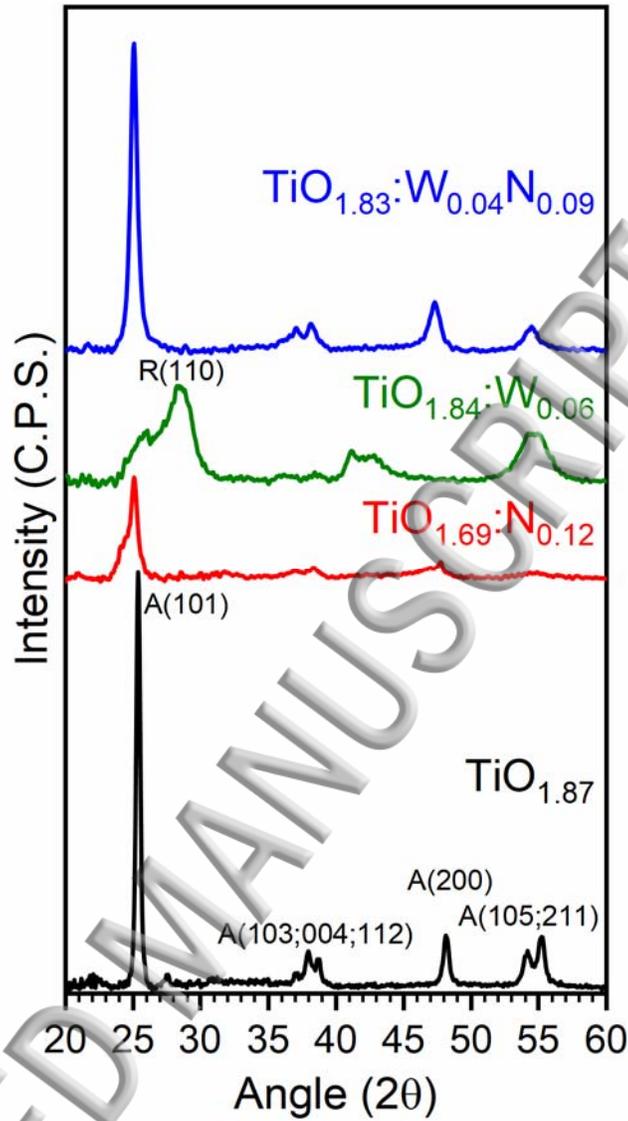
Figure 6: Typical XRD spectra of the sputter-deposited TiO_2, TiO_2:N, TiO_2:W, and TiO_2:WN films.
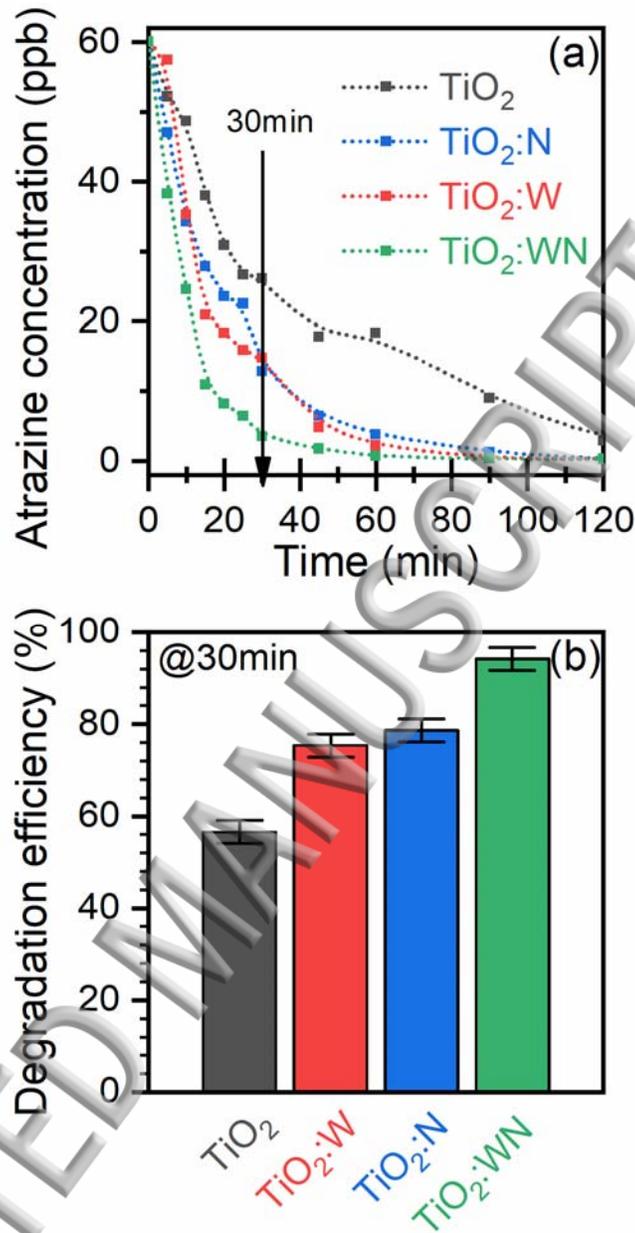
Figure 7: (a) Residual Atrazine concentration as a function of EPC degradation time, and (b) electro-photocatalytic degradation efficiency of atrazine, under AM1.5 solar irradiation, for the four different photoanodes (i.e. TiO_2, TiO_2:N, TiO_2:W, and TiO_2:WN thin-films).

(a) $W_{power} \uparrow @R_{N2} = 6\%$

Tungsten Power W_{power} (mW/cm^2)

Deposition Rate (nm/min)

$R_{N2} \uparrow @W_{power} = 132$mW/cm^2
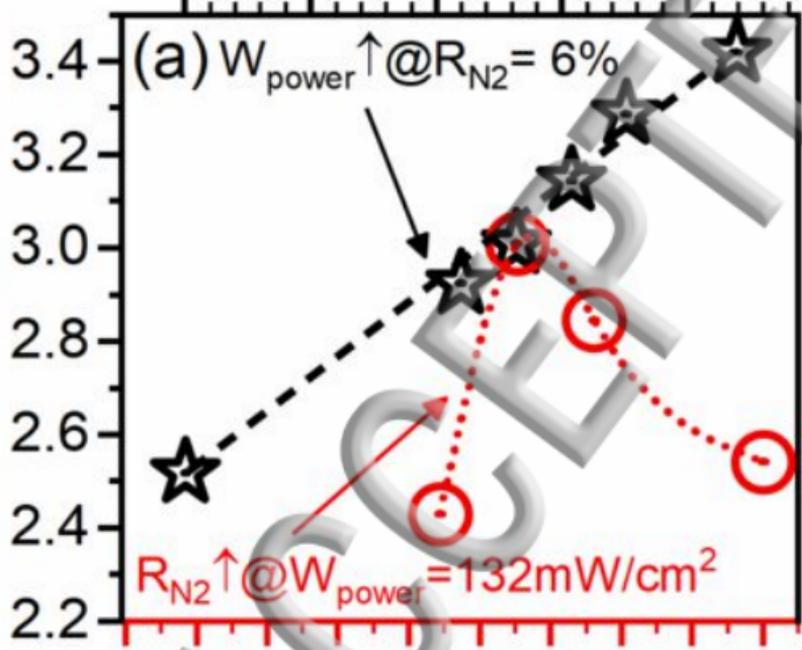
Nitrogen Flow Rate Ratio R_{N2} (%)

(b)

TiO$_2$:W,N 400nm

Si substrate

(a) $W_{power} = 132 mW/cm^2$

(b) $R_{N2} = 6\%$

O 1s | Ti 2p | N 1s | W 4f & Ti 3p

TiO$_2$:WN

TiO$_2$:W

TiO$_2$:N

TiO$_2$

Counts (Arb. Units)

Binding Energy (eV)

Labels in figure: O$^{(W)}$, O$^{(TiII)}$, O$^{(TiIII)}$, O$^{(TiIV)}$, O$^{(H)}$, Ti^{II}, Ti^{III}, Ti^{IV}, N^{Sub}, N^{Inter}, W^{VI}, W^{IV}, 1/2, 3/2

Figure (a): Transmittance (abs) vs Energy (eV).

- Undoped
- W-doped
- N-doped
- (WN)
- ×2
- ×2
- ×50

Figure (b): Tauc Plot $(\alpha * h * \upsilon)^{1/2}$ vs Energy (eV).

- $E_g \sim 3.2$ eV
- $E_g \sim 2.3$ eV (N)
- $E_g \sim 3.2$ eV (W)
- $E_g \sim 2.3$ eV (WN)

Band Gap (eV)

$TiO_{1.83}:W_{0.04}N_{0.09}$

R(110)

$TiO_{1.84}:W_{0.06}$

$TiO_{1.69}:N_{0.12}$

A(101)

$TiO_{1.87}$

A(103;004;112)

A(200)

A(105;211)

Intensity (C.P.S.)

Angle (2θ)